Mesozoic 001 (3): 420–432
https://www.mapress.com/mz/

Article

ISSN 3021-1859 (print edition)
MESOZOIC
ISSN 3021-1867 (online edition)

https://doi.org/10.11646/mesozoic.1.3.21
http://zoobank.org/urn:lsid:zoobank.org:pub:C91D154F-F7A2-417F-8A89-7F5AA3838329

Influence of climate and marine transgression on Mesozoic–Cenozoic diagenesis of clastic rocks in the Tabei Uplift, Tarim Basin, China

SHI-JIE ZHANG[1, 2, *], YONG-QIANG ZHAO[2], YUAN-ZHUANG CHEN[3], BIN ZHANG[4], YI-WEI XU[5], HONG-QIANG MA[2], YONG-TAO XIA[6], JIA-YUAN CAO[1], YU-YANG YU[1] & LI-QIN HAN[1]

[1]*College of Tourism, Henan Normal University, Xinxiang 453007, China*
[2]*Wuxi Research Institute of Petroleum Geology, Sinopec Petroleum Exploration and Production Research Institute, Wuxi 214126, China*
[3]*Northwest Exploration Research Center, Sinopec Petroleum Exploration and Production Research Institute, Beijing 100083, China*
[4]*Mineral Resources Exploration Center of Henan Geological Bureau, Zhengzhou 450012, China*
[5]*Nanjing Institute of Geology and Palaeontology, Chinese Academy of Sciences, Nanjing 210008, China*
[6]*Petroleum Exploration and Development Research Institute, Northwest Oilfield Company, Sinopec, Urumchi 830011, China*

zhangshijiex@foxmail.com; https://orcid.org/0000-0002-6973-493X
zhaoyq.syky@sinopec.com; https://orcid.org/0009-0000-2591-3162
chenyz.syky@sinopec.com; https://orcid.org/0009-0002-5603-1319
zhangbin2602@163.com; https://orcid.org/0009-0008-2619-1964
kongjuzixing@126.com; https://orcid.org/0000-0002-3387-7453
mahq.syky@sinopec.com; https://orcid.org/0009-0008-7063-8604
xiayt.xbsj@sinopec.com; https://orcid.org/0009-0006-7082-8024
jiayuancao@163.com; https://orcid.org/0009-0006-7665-6569
yuyuyangg@qq.com; https://orcid.org/0000-0002-6346-8909
hanliqin@lzb.ac.cn; https://orcid.org/0009-0004-4956-3178
**Corresponding author*

Abstract

The Mesozoic–Cenozoic clastic rocks in the Tabei Uplift form one of the most hydrocarbon-rich zones in the Tarim Basin of China. Understanding how diagenesis has affected the petrophysical properties of the sandstone is crucial for developing regional exploration strategies. Although most studies have investigated the physical conditions during sedimentation and chemical processes during diagenesis, the hydrochemical environment during sedimentation and subsequent diagenesis has received little attention. This study employed petrographic observations, paleo-geothermal reconstructions, and paleoenvironmental analysis to constrain the regional climatic conditions, hydrochemical environment of deposition, and diagenetic features of clastic rocks in the Tabei Uplift. The sandstone at depths of 3500–6000 m is located mainly in the A phase of the middle diagenetic stage, and exhibits three types of diagenesis. Triassic–Jurassic sandstones are dominated by silica, kaolinite, and chlorite cements, Cretaceous sandstones by mainly carbonate cements, and Paleogene sandstones by carbonate and evaporite cements. These diagenetic stages correspond to paleoclimatic changes during the earliest Late Jurassic and the maximum marine transgressions of the Proto-Tethys during the Paleogene, thereby highlighting the influence of climatic change and transgressions on the water conditions during deposition and the type of diagenesis.

Keywords: Tarim Basin, diagenesis, Mesozoic–Cenozoic, paleoenvironmental change, sedimentary aqueous media

Introduction

The Tarim Basin is the largest petroliferous sedimentary basin in China. The Tabei Uplift in the northern part of the basin is a structural unit containing large accumulations of oil and gas (Xu *et al*., 2004; Jin *et al*., 2008). In recent decades, efforts to explore lithological and stratigraphic traps in the Mesozoic–Cenozoic clastic rocks in the Tabei Uplift have intensified (Jia & Pang, 2015; Yang *et al*., 2020); however, the exploration results remain disappointing. As the burial depth increases, the heterogeneity of the rock properties also increases, and some target areas have poor reservoir development, which makes identification of effective traps challenging (Gu *et al*., 2002; Morad *et al*., 2010; Jia & Pang, 2015; Zhang *et al*., 2019; Sun *et al*., 2020). As such, studies of diagenesis are needed to understand the controls on variations in sandstone petrophysical properties, which can then be used to optimize regional exploration strategies (Zhu *et al*., 2007; Ajdukiewicz & Lander, 2010; Luo *et al*., 2020; Yang *et al*., 2020; Xia *et al*., 2024).

Sandstone diagenesis is affected primarily by the supply of clastic sediment from the source area, the physical and chemical features of the depositional environment, and the diagenetic stage (Bjørlykke, 1983, 2014; Fuchtbauer, 1983; Li *et al*., 2006; Xie *et*

 Submitted: 19 Sept. 2024; accepted by D.-Y.Huang: 27 Sept. 2024; published: 30 Sept. 2024

al., 2009; Morad *et al*., 2010). Diagenetic studies of Mesozoic–Cenozoic clastic rocks in the Tarim Basin have focused on the sedimentary facies, reservoir classification and petrophysics, and effects of burial on diagenesis, with particular attention to the physical conditions during sedimentation and chemical processes during diagenesis (Zhu *et al*., 2007; Zhang *et al*., 2018a; Zhang *et al*., 2019; Sun *et al*., 2020; Yang *et al*., 2020; Xia *et al*., 2024). However, there has been little research on the chemical characteristics of the water body during sedimentation and its implications for diagenesis (Fuchtbauer, 1983; Li *et al*., 2006; Han *et al*., 2009; Xie *et al*., 2009; Luo *et al*., 2020). The Tabei Uplift experienced significant paleoclimatic changes and transgressive–regressive cycles during the Mesozoic–Cenozoic (Hendrix, 1992; Tang *et al*., 1992; Zhou, 2001; Li *et al*., 2004; Zhang *et al*., 2018b; Yi *et al*., 2019), resulting in marked variations in water chemistry in the sedimentary depositional environment (Fuchtbauer, 1983; Zheng & Ying, 1997; Ying *et al*., 2003; Li *et al*., 2006; Xie *et al*., 2009). These variations are expected to have affected the types and processes of diagenesis (Bjørlykke, 1983; Zheng & Ying, 1997; Ying *et al*., 2003; Li *et al*., 2006; Han *et al*., 2009; Xie *et al*., 2009), but this has been little studied, which limits our understanding of diagenesis in the Tabei Uplift.

This study investigated the Mesozoic–Cenozoic clastic rocks in the Tabei Uplift, China (Fig. 1). Petrographic analysis was used to identify the sandstone types, cements, and porosity. Diagenetic stages were determined using vitrinite reflectance (Ro), fluid inclusion homogenization temperatures, and smectite contents of mixed-layer illite/smectite. Paleoenvironmental changes were determined from trace element data and the clay minerals in mudstones. Our findings reveal three types of diagenetic characteristics in the Triassic–Jurassic, Cretaceous, and Paleogene sediments, primarily driven by climatic changes and marine transgressions.

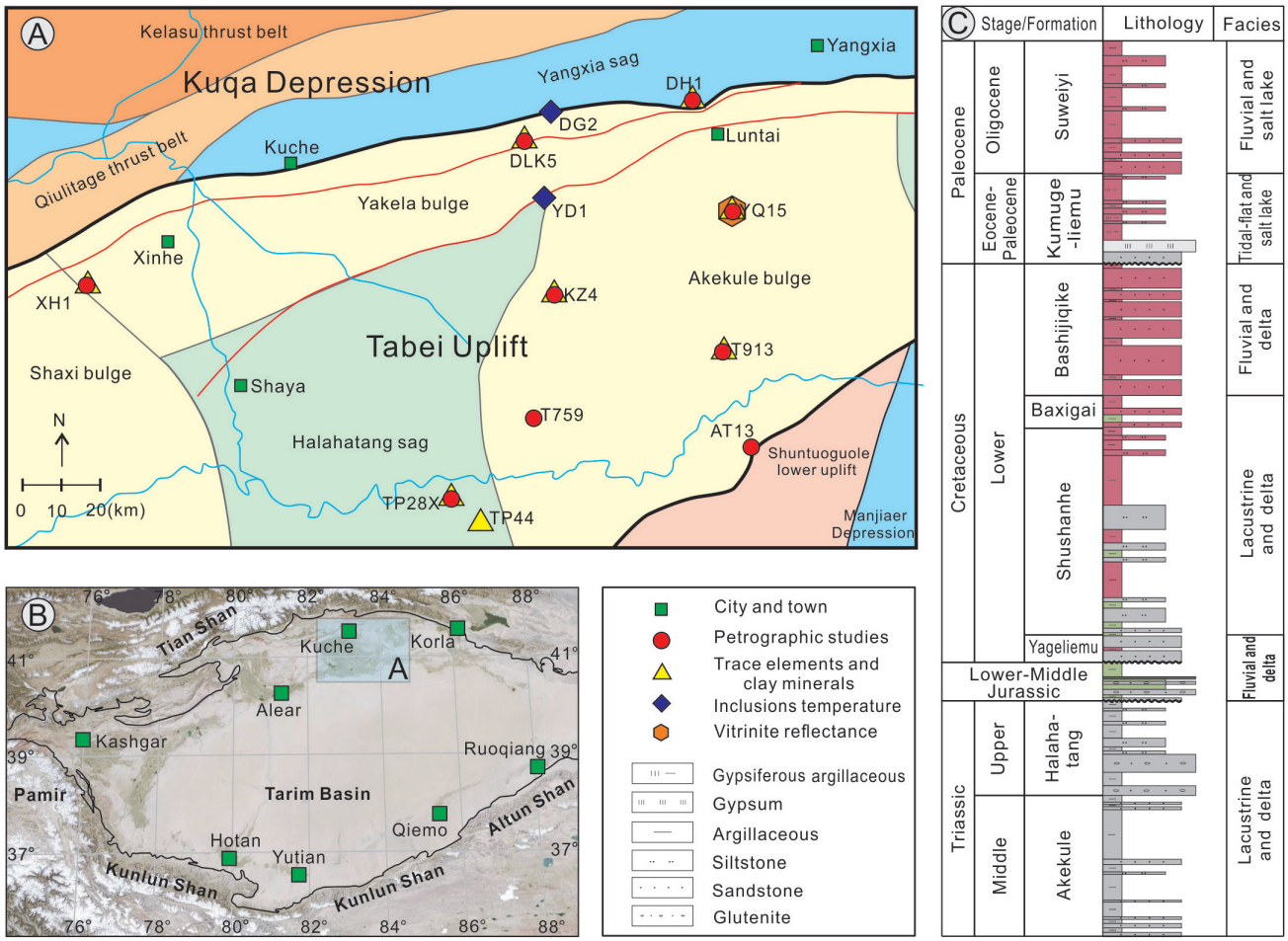

FIGURE 1. Geology of the study area. **A**, Simplified map of the major tectonic units within the northern Tarim Basin, modified from Qi *et al*. (2020), with the location indicated by the rectangle in **B**. The sampling locations of drillcore recovered from the Tabei Uplift and analytical methods are shown by symbols. **B**, Satellite image of the Tarim Basin and surrounding mountain belts (background image is from Google Earth). **C**, Typical sedimentary log and lithostratigraphic divisions of Triassic–Paleocene strata in the Tabei Uplift, after Qi *et al*. (2020).

Geological setting

The Tabei Uplift is an E–W-trending paleo-uplift located in the northern Tarim Basin (Fig. 1). It is bound to the east by the Kuruktag Block, to the west by the Awati Depression, to the north by the Kuqa Depression, and transitions into the Northeast Depression via a slope. The Tabei Uplift extends *ca*. 480 km from east to west and 70–110 km from north to south, covering an area of *ca*. 3.66 × 10^4 km^2 (Liu *et al*., 2014). The strata range from Sinian to Cenozoic in age (Zhou, 2001). Paleozoic to Mesozoic strata thin from south to north, whereas Cenozoic strata thin from north to south (Qi *et al*., 2020).

The Triassic–Jurassic strata in the Tabei Uplift occur on either side of the paleo-uplift (Wu *et al*., 2019). The Triassic strata are subdivided into the Ketuer Formation (T_1k), Akekule Formation (T_2a), and Halahatang Formation (T_3h) (from bottom to top; Fig. 1C; Zhou, 2001). These strata are gray clastic rocks with coal seams and thin coal beds. The sedimentary environment was a lacustrine setting under humid climatic conditions (Compiling Group for Xinjiang Regional Stratigraphic Chart, 1981; Hendrix, 1992; Liu *et al*., 2014). The Lower–Middle Jurassic sediments are bound by unconformities (Wu *et al*., 2019) and consist of gray conglomerates, sandstones, mudstones, and coal beds. Deposition occurred in braided river deltaic and lacustrine facies (Zhou, 2001; Liu *et al*., 2014).

The Lower Cretaceous sediments consist of brown–red clastic rocks that overlap onto and cover the Tabei Uplift (Wu *et al*., 2019; Xia *et al*., 2024). They form a coarse-fine-coarse sequence up-section, and are subdivided into the Yageliemu Formation (K_1y), Shushanhe Formation (K_1s), Baxigai Formation (K_1b), and Bashijiqike Formation (K_1bs) (Compiling Group for Xinjiang Regional Stratigraphic Chart, 1981; Liu *et al*., 2014). Upper Cretaceous sediments are absent in the central–northern part of the Tarim Basin (Wu *et al*., 2019). Abundant continental red beds and palynomorph assemblages (Li *et al*., 2019) demonstrate this area was dominated by lacustrine and fluvial deltaic facies under relatively arid climatic conditions (Fig. 1C; Liu *et al*., 2014; Zhang *et al*., 2018a; Qi *et al*., 2020).

The Paleocene–Eocene Kumugeliemu Group ($E_{1-2}km$) and Oligocene Suweiyi Formation (E_3s) consist of gypsum, siltstones, sandstones, and scarce conglomerates and limestones (Fig. 1C; Zhou, 2001). The gastropod assemblage and sulfur isotopic composition of the gypsum layer above the basal conglomerates indicate this area was affected by a marine transgression during the early Cenozoic (Tang *et al*., 1992; Zhou, 2001; Xu *et al*., 2020). The gypsum-bearing clastic rocks indicate the depositional environment was dominated by fluvial, lacustrine, and salt lake facies under arid climatic conditions (Fig. 1C; Chen *et al*., 2017; Qi *et al*., 2020).

Material and methods

This study examined rock and cast thin-sections, and scanning electron microscopy images of 21 Mesozoic–Cenozoic sandstone samples from the Tabei Uplift to determine the sample petrography, cements, and porosities (Fig. 1A). We obtained vitrinite reflectance (Ro) values, fluid inclusion homogenization temperatures, and the proportion of smectite in mixed-layer illite/smectite to quantify the paleo-temperatures. The diagenetic stage was determined based on the *Division of Clastic Diagenetic Stage* established by the petroleum and natural gas industry standards of the People's Republic of China (SY/T 5477-2003) (Ying *et al*., 2003). Ro measurements of two samples from well YQ15 (Fig. 1A) and scanning electron microscopy imaging were undertaken at the Beijing UniOil Technology Company, Beijing, China. Fluid inclusion temperatures of five samples from wells DG2 and YD1 (Fig. 1A) were determined with a THMS 600G heating–freezing stage (Linkam, UK) at the China University of Geosciences, Wuhan, China.

Trace element data and the clay mineralogy for 30 mudstone samples were used to quantitatively evaluate the sediment provenance, source weathering intensity, and redox state of the depositional environment (Fig. 1A; Singer, 1984; McLennan, 2001; Muhs *et al*., 2001; Tribovillard *et al*., 2006). Trace and rare earth elements (REEs) were analyzed with a NexION 300D inductively coupled plasma–mass spectrometer (ICP–MS). Clay mineral X-ray diffraction (XRD) analysis was conducted with an X'Pert PRO MPD XRD system (Panalytical; Netherlands) at the Analytical Laboratory of the Beijing Research Institute of Uranium Geology (BRIUG), China.

Results

Sandstone petrography, cement, and porosity

The Triassic samples are feldspathic-quartzose-lithic sandstones, with lithic fragments exceeding 50 vol.%. The Jurassic, Cretaceous, and Paleogene sandstones contain similar clastic components (Figs 2, 3). The only Jurassic sample is a lithic-quartzose sandstone. Cretaceous samples are dominantly feldspathic-lithic-quartzose sandstones. The Paleogene samples are mainly feldspathic-quartzose sandstones. The rock fragments in all samples are predominantly silicic volcanic rocks

(Fig. 2). Metamorphic rock fragments are relatively scarce, but are primarily quartzite, and scarce sedimentary rock fragments occur in some samples.

The Mesozoic–Cenozoic sandstones contain three types of cement (Figs 2, 4, 5). Triassic–Jurassic samples are cemented mainly by authigenic kaolinite, chlorite, and quartz, with abundant quartz overgrowths. Authigenic kaolinite has a book-like form and occurs between detrital grains, while authigenic chlorite has a blade-like form on grain surfaces. Cretaceous samples are characterized by carbonate cements (Fig. 2B, C). Paleogene samples are also primarily carbonate-cemented, but locally contain gypsum and anhydrite cements (Fig. 2A).

The porosity of the sandstone samples ranges from 0% to 15% (area percentage in cast thin-sections), with an average of 7.14% (Figs 6, 7). Two samples of the Shushanhe Formation contain carbonate cements that occupy nearly all the intergranular pores (Figs 2C, 7A). The average porosity is 7.1% for the four Triassic–Jurassic samples, 7.2% for the twelve Cretaceous samples, and 6.9% for the five Paleogene samples. The main pore types include intergranular dissolution (54.2%) and primary intergranular (27.3%) pores, followed by residual intergranular (11.5%) and intragranular dissolution (4.2%) pores. Micro-pores and micro-fractures were not well-developed, and account for 2.8% of the total porosity (Fig. 6).

Clay minerals and trace elements

Kaolinite and chlorite in the Middle Triassic–Lower Jurassic mudstones make up 12.5% and 9.1% of the total clay minerals, but just 3.0% and 5.8% in the post-Jurassic samples, respectively (Fig. 8). Moreover, the chlorite contents of two samples from the base of the

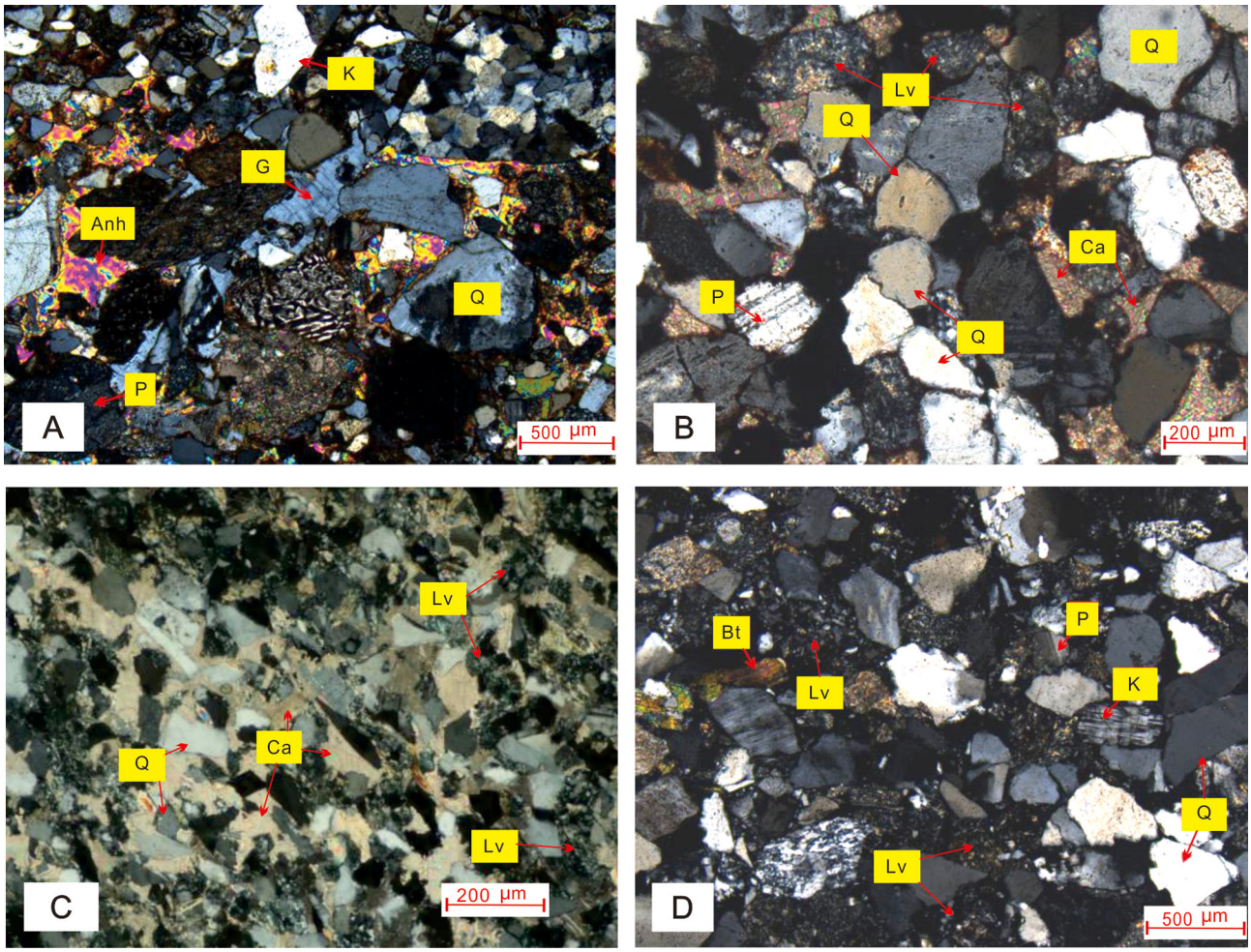

FIGURE 2. Typical photomicrographs of Mesozoic–Cenozoic sandstone in the Tabei Uplift. **A**, DH1 well, 5232.30 m, Paleogene Suweiyi Formation, unequal-grained lithic–feldspathic–quartzose sandstone, gypsum and anhydrite filling intergranular pores can be seen. **B**, DH1 well, 5717.40 m, Lower Cretaceous Baxigai Formation, feldspathic–lithic–quartzose sandstone, the intergranular pores are filled by calcite cements, and the lithic fragments are dominated by felsic volcanic clasts, **C**, XH1 well, 5691.40 m, Lower Cretaceous Shushanhe Formation, feldspathic–lithic–quartzose siltstone, all intergranular pores are filled by calcareous cementation, and areal porosity is 0. **D**, AT13 well, 4414.63 m, Middle Triassic Akekule Formation, feldspathic–quartzose–lithic sandstone, cements are siliceous and clay minerals, and the lithic fragment types are dominated by felsic volcanic clasts. Anh, anhydrite; G, gypsum; Q, quartz; K, potassium feldspar; P, plagioclase; Lv, volcanic fragment; Bt, biotite; Ca, calcite.

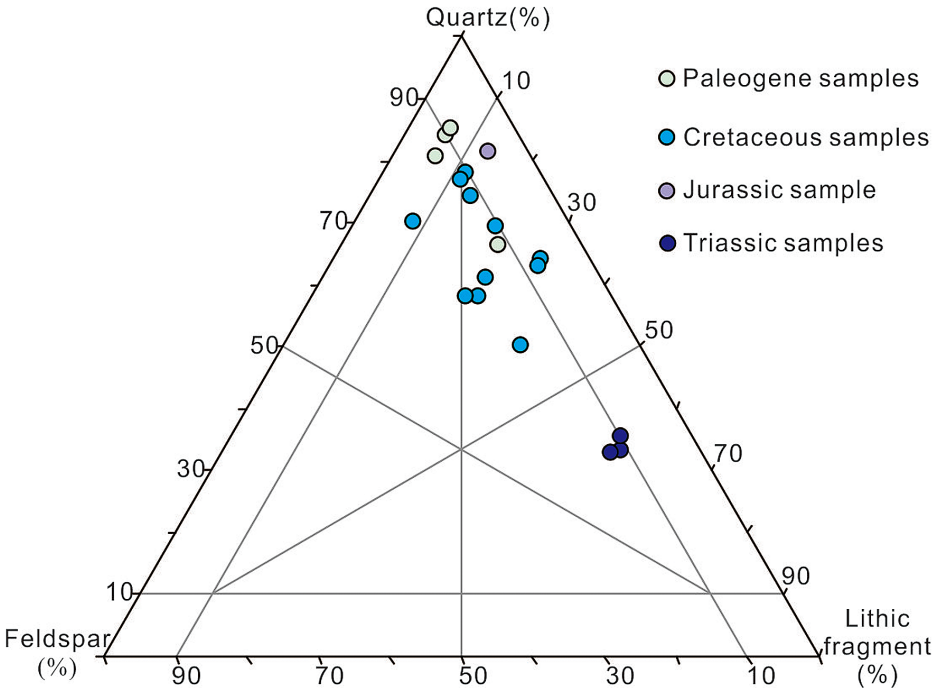

FIGURE 3. The triangle diagram of detrital composition in the Mesozoic–Cenozoic sandstone of the Tabei Uplift. The classification and nomenclature is based on the Garzanti (2019).

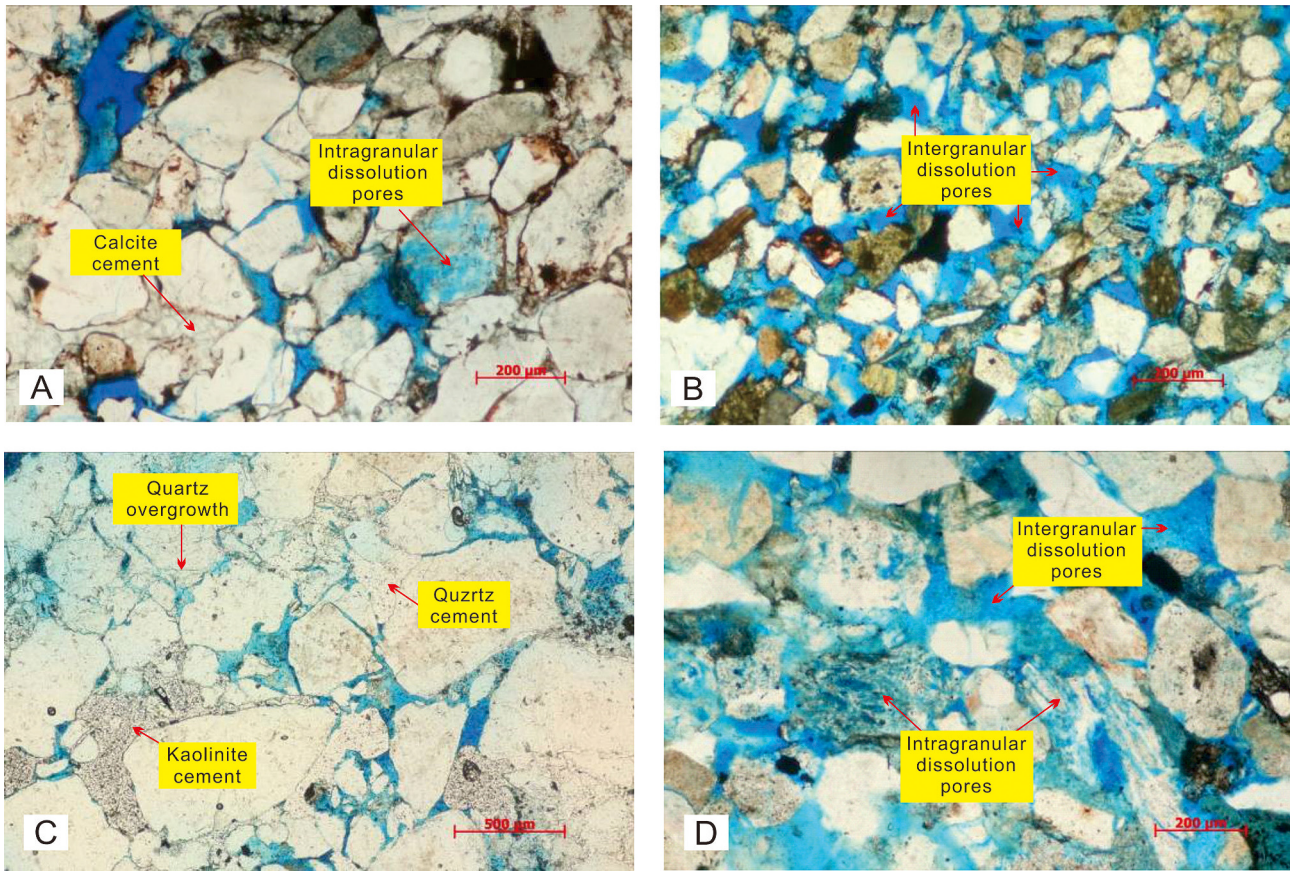

FIGURE 4. The typical photographs of the cast thin sections. **A**, DH1 well, 5232.30 m, Lower Cretaceous Baxigai Formation, line contact, calcite cementation and dissolution of feldspar and lithic fragment can be seen. **B**, TP28X well, 3694.10 m, Lower Cretaceous Shushanhe Formation, with point contact, low content of cement and relatively developed pores. **C**, YQ15 well, 4909.20 m, Lower Cretaceous Yageliemu Formation, dominant by line contact, cements are quartz and kaolinite. **D**, YQ15 well, 5108.86 m, Upper Triassic Halahatang Formation, intragranular dissolved pores of lithic fragment and feldspar can be seen.

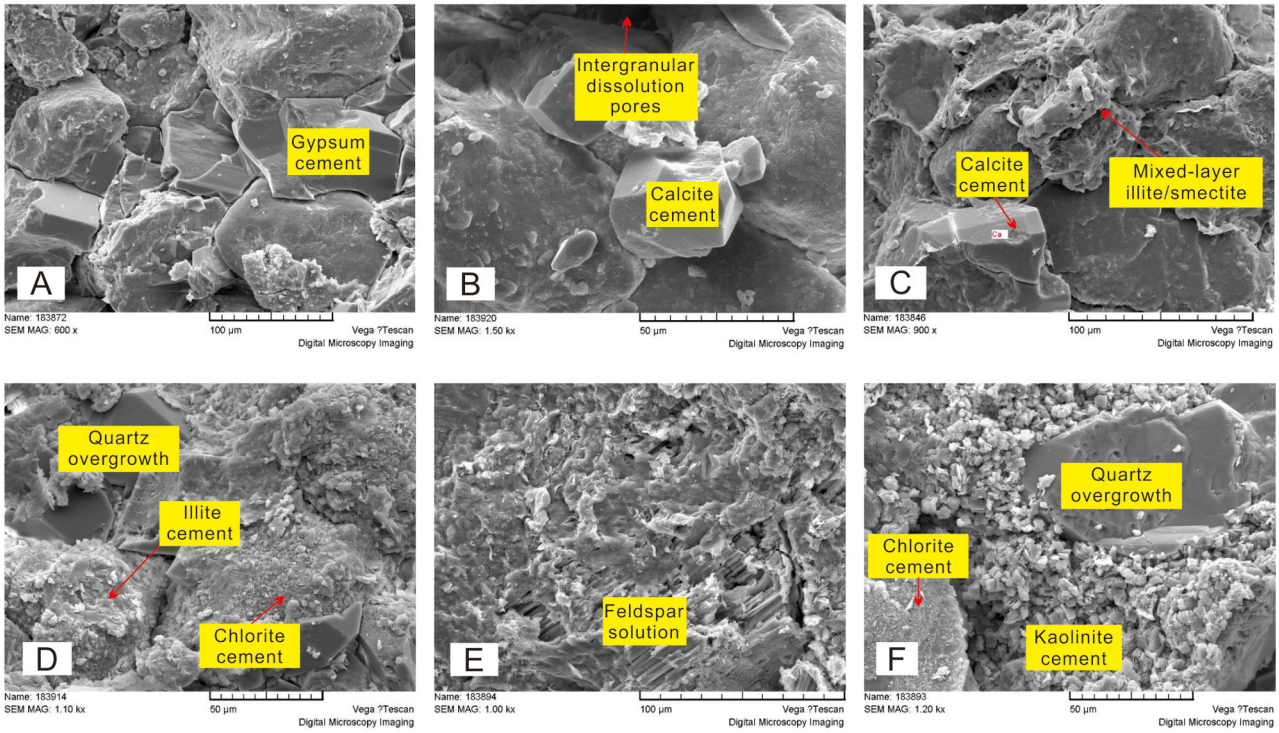

FIGURE 5. The microscopic feature of Mesozoic–Cenozoic sandstone in the Tabei Uplift under scanning electron micrographs. **A**, XH1 well, 4954.00 m, Paleogene Suweiyi Formation, intergranular pores are filled by gypsum cementation. **B**, YQ15 well, 3766.60 m, Paleogene Kumugeliemu Group, calcite cementation. **C**, TP28X well, 3694.10 m, Lower Cretaceous Shushanhe Formation, cements are calcite and mixed-layer illite/smectite. **D**, XH1 well, 5691.40 m, Lower Cretaceous Shushanhe Formation, the intergranular ferrodolomite cements, quartz overgrowth, and illite and chlorite on the surface of grains can be seen. **E**, YQ15 well, 5103.20 m, Upper Triassic Halahatang Formation, feldspar dissolution. **F**, YQ15 well, 5103.20 m, Upper Triassic Halahatang Formation, quartz overgrowth, chlorite on the surface of grains, and intergranular kaolinite can be seen,

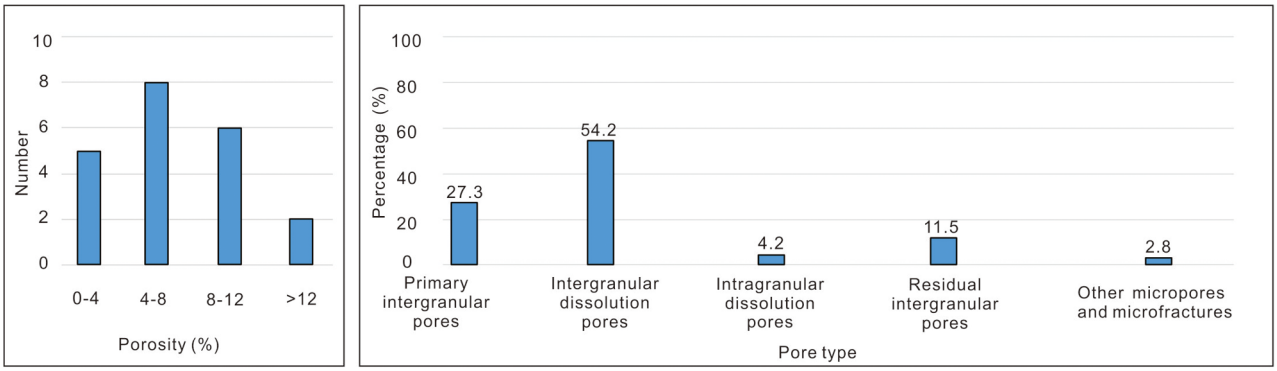

FIGURE 6. Statistics of the porosity (area percentage) and pore type in the Mesozoic–Cenozoic sandstone of the Tabei Uplift.

Cretaceous Kapushaliang Group are much higher than the average value. However, the contents of mixed-layer illite/smectite exhibit the opposite trend to kaolinite and chlorite, with an average content of 55.8% in the Middle Triassic–Lower Jurassic mudstones, and >63% in the post-Jurassic samples. There is no obvious change in illite content, and the smectite content is below the detection limit.

The ratios of immobile trace elements (*e.g.*, Y/Sc) are similar in the Middle Triassic–Cretaceous strata and Suweiyi Formation mudstones, but differ from those of the Kumugeliemu Group (Fig. 8). This difference is not evident for Ba/Sr and V/Ni values. The Ba/Sr values of the Cretaceous–Paleogene mudstones are uniform, but much lower than those of the Middle Triassic–Lower Jurassic samples. Similarly, the V/Ni values of the Kumugeliemu Group mudstones are similar to those of the Kapushaliang Group and Suweiyi Formation, and lower than those of the Middle Triassic–Lower Jurassic samples.

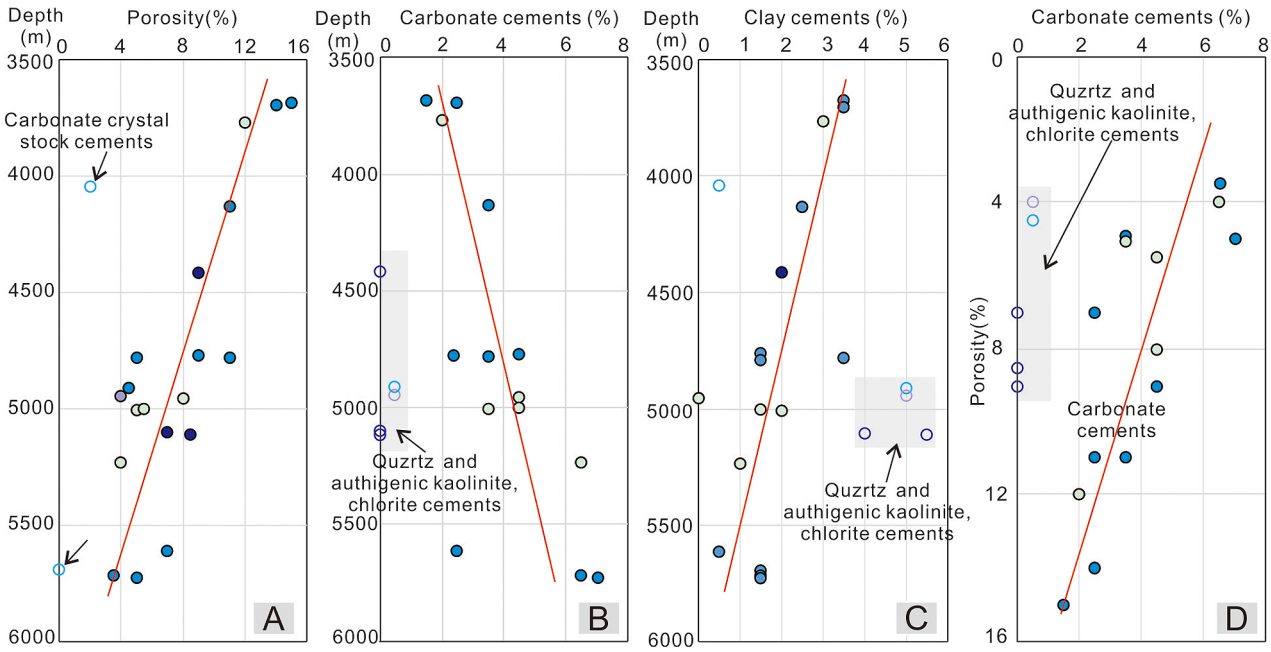

FIGURE 7. Scatter plots of depth versus porosity (**A**), carbonate cement content (**B**), clay mineral content (**C**), and correlation between porosity and carbonate content (**D**). The sampling stratigraphic units represented by different colors in the circle are shown in Fig. 3

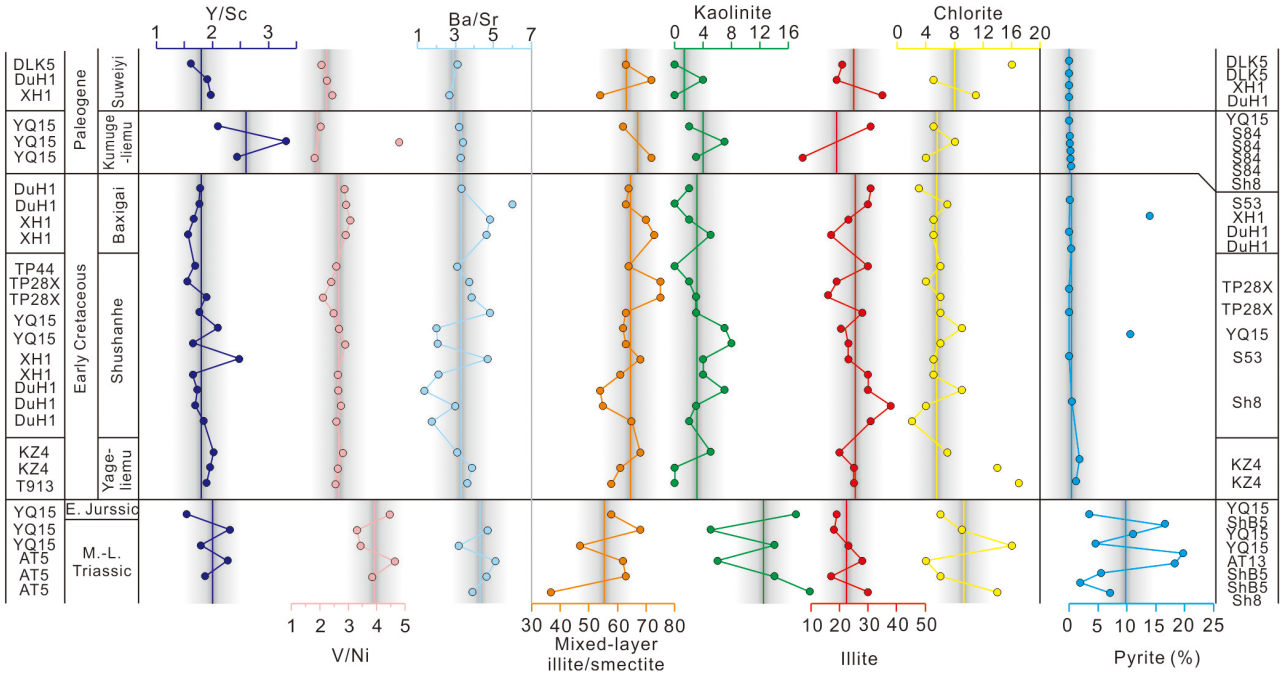

FIGURE 8. The ratio values of immobility trace elements (Y/Sc), of indicating redox conditions trace elements (V/Ni), of indicating weathering strength trace elements (Ba/Sr), and types and contents of clay minerals in Mesozoic–Cenozoic mudstones in the Tabei Uplift. The pyrite (%) means the pyrite content in the total heavy minerals in sandstones.

Vitrinite reflectance, fluid inclusion homogenization temperatures, and smectite contents

Both samples for vitrinite reflectance analysis were obtained from well YQ15. The sample from 4938 m depth has an average Ro value of 0.67% (n=30; standard deviation= 0.04). The sample from 5068 m depth has an average Ro value of 1.05% (n=25; standard deviation= 0.09) (Fig. 9).

The average homogenization temperatures for quartz-hosted fluid inclusions from two sandstone samples from well YD1 at 5339 m depth are 109–131 °C (n=19) and 115–131 °C (n=30). The sandstones from depths

TABLE 1. The average homogenization temperatures for quartz-hosted fluid inclusions.

Bore-hole	Depth (m)	Average homogenization temperature (°C)										Num-ber
		Brine inclusions				Hydrocarbon-bearing brine inclusions				Petroleum inclusions		
		Th1	Th2	Th3	Th4	Th1	Th2	Th3	Th4	Th2	Th3	
YD1	5339		109.5	126.5				126.8		113.7	131.1	19
	5339		119	131.2			114.9	126.1		115.2	126.3	30
DG2	6436	91.8	107.9	127.1	140.1			127.6	153.4			15
	6450	97.3	122.6	135	169.7	88.6		123.5				15
	6525	101.4	118	136.7					136.4			15

of 6434, 6450, and 6524 m in well DG2 have average homogenization temperatures of 91–153 °C (n=15), 88–169 °C (n=15), and 101–136 °C (n=15), respectively (Table 1).

Increased burial depth accelerates the conversion of smectite and illite/smectite to illite. This study quantitatively evaluated the diagenetic stage by calculating the average smectite contents in mixed-layer illite/smectite from adjacent depth intervals. The average smectite content is 23.8% for the depth range of 3542–3772 m. With increasing depth, the average smectite contents for the intervals of 4132–4226, 4769–5238, and 5610–5916 m are 23.5%, 14.1%, and 13.9%, respectively (Fig. 9).

Discussion

Diagenetic stages

The Ro values at depths of 4938 and 5068 m fall within the range for phase A of the middle diagenetic stage (0.5%–1.3%) (Ying *et al*., 2003). The homogenization temperatures of quartz-hosted fluid inclusions at depths of 5339–6524 m are consistent with the recommended paleo-temperature range of 85–140 °C for phase A. The recommended smectite contents in mixed-layer illite/smectite for phase A of the middle diagenetic stage are 50%–15%, whereas for phase B they are <15%. At depths of 4500–6000 m, the smectite content (*ca*.14%) in mixed-layer illite/smectite corresponds to the earliest phase of stage B of the middle diagenetic stage. The smectite contents in mixed-layer illite/smectite at depths of 3500–4500 m are *ca*. 23%, indicative of the late phase of stage A. Therefore, it is reasonable to classify the Mesozoic–Cenozoic sandstones in the depth range of 3500–6000 m as phase A of the middle diagenetic stage.

Variations in cement with depth

A clear linear correlation is evident between porosity and depth for the Mesozoic–Cenozoic sandstones from the Tabei Uplift (Fig. 7A). As the burial depth increases, the porosity decreases. Two samples deviate from this trend due to carbonate cement occupying nearly all the intergranular pore space (Fig. 2C). Although the cement types vary amongst the different stratigraphic units, these variations do not affect the observed trend (Fig. 7A). The sandstone grains at depths of 3500–4300 m are dominantly in point contact. At depths of 4300–5000 m, both point and line contacts are present, while below 5000 m depth, line contacts predominate (Figs 2, 4, 9). At the transition between point–line and line contacts, the grain framework becomes tightly packed. Further compaction results in negligible reduction in intergranular volume and porosity (Ajdukiewicz & Lander, 2010; Bjørlykke, 2014). This indicates that mechanical compaction at depths above 5000 m was a significant factor in porosity reduction.

Carbonate cements are only dominant in the Cretaceous–Paleogene sandstones (Fig. 7B). With increasing depth, the content of carbonate cement increases as porosity decreases, showing a strong linear correlation (Fig. 7A, D). Secondary quartz growth is common in the Mesozoic sandstones and intensifies with depth (Figs 4, 5). SEM images show widespread clean, angular quartz overgrowths. Below 5000 m depth, smaller authigenic quartz crystals occur in inter-grain pores. These observations indicate that the carbonate and quartz cements have reduced the sandstone porosity in this depth range.

The contents of authigenic clay minerals in the sandstones decrease with depth (Fig. 7C) from *ca*. 3.5% at 3600 m to *ca*. 0.5% at >5500 m. This trend is not observed for the Triassic–Jurassic samples, which have higher contents of clay minerals as compared with Cretaceous–Paleogene samples at equivalent depths. In addition, dissolution of feldspar and lithic fragments is observed in thin-sections and SEM images of Triassic–Jurassic sandstones, although the related increase in porosity is minimal (Figs 4–6).

Three types of diagenesis

Observations of rock and cast thin-sections, and scanning electron microscopy images (Figs 2, 4, 5), along with plots

of depth versus porosity (Fig. 7), enable the identification of three types of diagenesis in the Mesozoic–Cenozoic sandstones of the Tabei Uplift (Fig. 9). Silica, kaolinite, and chlorite are the main cements in the Triassic–Jurassic sandstones (Figs 5F, 9). This is evident from secondary quartz growth, as is apparent in thin-sections, and widespread clean, angular quartz overgrowths in SEM images. Authigenic kaolinite occurs between grains, while authigenic chlorite occurs on grain surfaces, commonly accompanied by feldspar dissolution (Figs 4D, 5E).

Carbonates are the predominant cement in the Cretaceous sandstones, followed by illite and mixed-layer illite/smectite (Figs 2B, C, 4A, 5B–D). The content of carbonate cement increases with depth (Fig. 7B), whereas the content of clay minerals decreases (Fig. 7C). Authigenic kaolinite and chlorite cements were only occasionally observed. Quartz and feldspar overgrowths were observed in SEM images (Fig. 5D), but feldspar dissolution is rare (Fig. 9).

Carbonates are the main cement in the Paleogene sandstones, but gypsum and anhydrite cements also occur locally (Figs 2A, 5A, B). In contrast to the Cretaceous samples, the Paleogene sandstones contain less authigenic kaolinite and chlorite, and infrequent quartz overgrowths (Fig. 9).

Depositional environments and changes in hydrochemistry

The sandstones in the Tabei Uplift are all within the same diagenetic stage, but the cement types and relative contents in the different stratigraphic units revealed three diagenetic types (Fig. 9). We suggest that the physical and chemical conditions during sedimentation, rather than the diagenetic stage, were the main control on the diagenetic type.

The kaolinite decreased and mixed-layer illite/smectite increased rapidly in mudstones during the Late Jurassic (Fig. 8), suggesting a significant climatic change (Singer, 1984; Hendrix, 1992; Li *et al*., 2004; Yi *et al*., 2019). Concurrently, the Ba/Sr ratio exhibits a marked decrease, indicating a rapid decrease in weathering intensity during the Late Jurassic (Muhs, 2001), followed by a period of stability. However, the Y/Sc ratios were uniform throughout the Mesozoic, implying the Late Jurassic was the time of a transition from a humid to an arid climate rather than a change in sediment provenance (McLennan, 2001).

The pyrite in the Triassic–Middle Jurassic sandstones accounts for 10% of the total heavy mineral content, but is scarce in the post-Jurassic samples (Fig. 8). The V/Ni ratio, which is a proxy for redox conditions (Tribovillard,

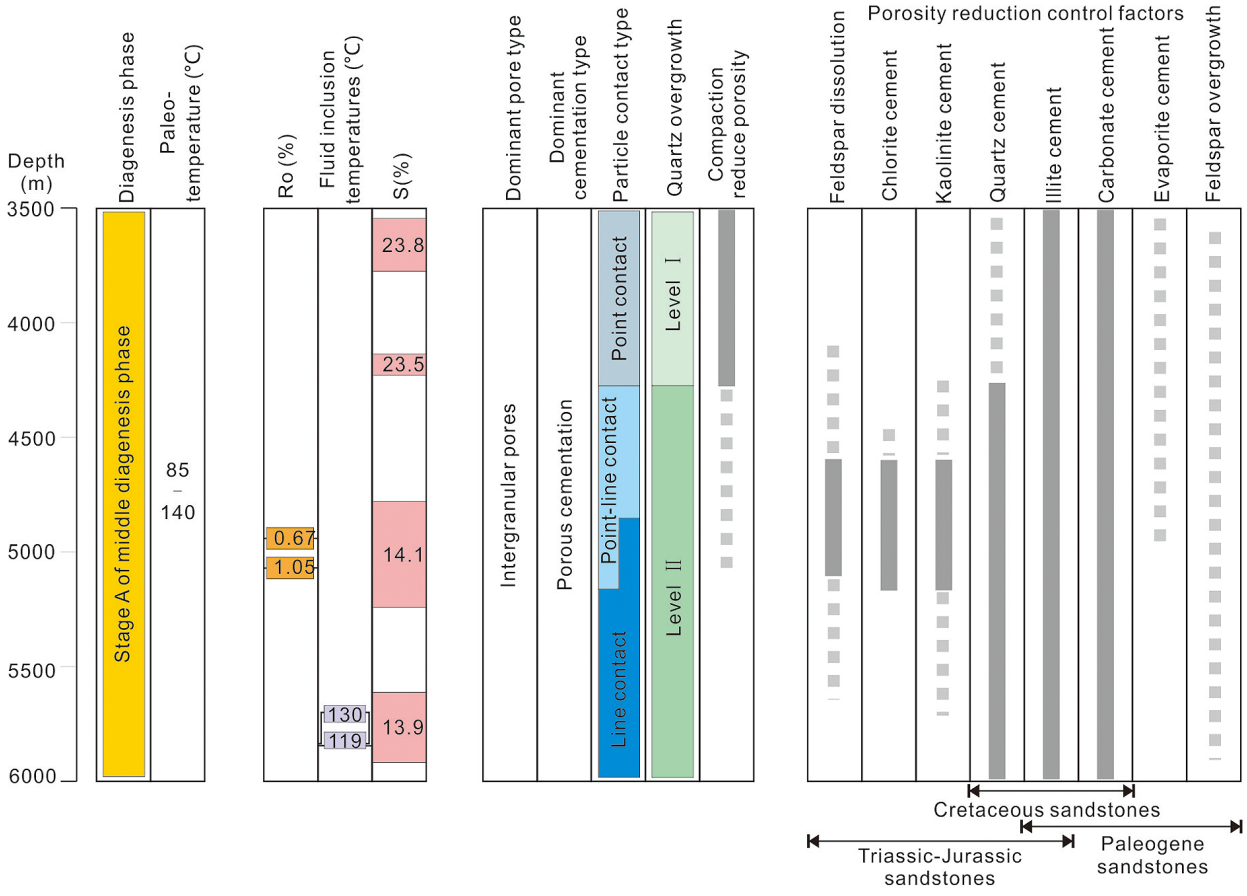

FIGURE 9. Synthesis of diagenetic stages and diagenetic characteristics of the Mesozoic–Cenozoic sandstone in the Tabei Uplift.

2006), exhibits a marked decrease during the Late Jurassic (Fig. 8). This indicates that changes in the pyrite contents were not due to provenance changes, but rather to a rapid change in the depositional environment from reducing to oxidizing conditions (Tribovillard, 2006). Regionally, Central Asia underwent a facies transition from Triassic–Middle Jurassic swamp to Cretaceous lacustrine facies (Hendrix, 1992; Tang *et al*., 1992; Zhou, 2001; Li *et al*., 2004; Zhang *et al*., 2018a; Yi *et al*., 2019; Qi *et al*., 2020), further indicating that the Triassic–Middle Jurassic was characterized by reducing depositional conditions and acidic water (Zheng *et al*., 1997).

The Ba/Sr ratios of the Cretaceous–Paleogene mudstones are uniformly low, indicating a consistently low intensity of weathering (Fig. 8). Lower–Middle Jurassic coal-bearing strata are absent during this period (Compiling Group for Xinjiang Regional Stratigraphic Chart, 1981; Zhou, 2001; Yang *et al*., 2017). The low kaolinite contents are consistent with the sporopollen assemblages (Li *et al*., 2004), which indicate an arid to semi-arid climate. The Cretaceous–Paleogene strata are predominantly reddish brown clastic rocks (Compiling Group for Xinjiang Regional Stratigraphic Chart, 1981; Zhou, 2001), with no pyrite and low V/Ni ratios (Fig. 8), reflecting a more oxidizing sedimentary environment (Tribovillard, 2006). The Shushanhe and Baxigai formations contain abundant shallow-water lacustrine ostracods (Zhou, 2001), indicative of a sedimentary environment dominated by shallow lake and deltaic facies with fresh or brackish water (Ying *et al*., 2003; Han *et al*., 2009; Liu *et al*., 2014; Zhang *et al*., 2018a; Qi *et al*., 2020).

The Proto-Tethys reached a maximum marine transgression in Central Asia during the Paleocene–Eocene (Tang *et al*., 1992; Zhou, 2001; Zhang *et al*., 2018b). Carbonate formations were deposited from west of Kashgar to east of Hotan, and extended northeast into the Kuqa Depression (Tang *et al*., 1992; Zhang *et al*., 2018b; Xu *et al*., 2020). The base of the Kumugeliemu Formation in the Tabei Uplift and Kuqa Depression is characterized by interbedded marine gypsum and bioclastic limestone (Tang *et al*., 1992; Xu *et al*., 2020). The Ba/Sr and V/Ni ratios, and clay minerals (Fig. 8) indicate stable arid climatic conditions at this time (Li *et al*., 2004), when the Tabei Uplift was dominated by tidal flat and saline lake facies with alkaline waters (Tang *et al*., 1992; Ying *et al*., 2003; Liu *et al*., 2014; Qi *et al*., 2020).

Influence of climate and marine transgression on diagenesis

The Triassic–Jurassic coal-bearing strata generated large amounts of humic acids and carbon dioxide during the early diagenetic stage, which dissolved interstitial carbonate (Zheng & Ying, 1997; Ying *et al*., 2003). Consequently, the Triassic–Jurassic and some lower Yageliemu Formation sandstones lack carbonate cement (Fig. 4C). Humic acid also dissolves silicate minerals and accelerates feldspar dissolution (Bjørlykke, 1983; Li *et al*., 2005). The dissolution of K- and Na-feldspar promoted the precipitation of kaolinite and release of silica, which facilitated secondary quartz overgrowths (Li *et al*., 2005). Increasing burial depth accelerated the conversion of smectite and illite/smectite to illite, which is a K-depleting reaction that further promoted the dissolution of K-feldspar and mica (Huang *et al*., 2009). This dissolution provided abundant Fe and Mg ions that facilitated chlorite formation (Tian *et al*., 2008). As such, the Triassic–Jurassic sandstones are cemented mainly by silica, kaolinite, and chlorite, and underwent widespread feldspar dissolution (Fig. 9).

The Cretaceous sediments are characterized by high-carbonate cement (Figs 2B, C, 5C), low contents of organic matter, and the absence of humic acids that would otherwise have dissolved the carbonate cement (Zheng & Ying, 2009). As the burial depth and temperature increased, the sandstones transitioned into the middle diagenetic stage, in which the carbonate solubility decreased, leading to gradual recrystallization (Yu & Lai, 2006). Consequently, calcite remained the dominant cement in these sandstones. Our results are consistent with simulations of multi-stage dissolution and support the view that carbonate cementation is a major factor in the degradation of sandstone porosity (Zhang *et al*., 2019; Xia *et al*., 2024).

The alkaline waters in the Paleogene saline lake in the Tabei Uplift promoted quartz dissolution and inhibited feldspar dissolution (Qiu *et al*., 2001; Ying *et al*., 2003). The reduced dissolution of feldspar further suppressed the formation of kaolinite and chlorite (Tian *et al*., 2008; Huang *et al*., 2009). Consequently, the Paleogene sandstones have fewer quartz overgrowths and contain little authigenic kaolinite and chlorite as compared with the Cretaceous sandstones (Fig. 9).

Conclusion

This study investigated the Mesozoic–Cenozoic clastic rocks in the Tabei Uplift of the Tarim Basin in China and determined the diagenetic stages and types, as well as the paleoclimatic and paleoenvironmental conditions during sediment deposition. The main conclusions are as follows.

1) The Mesozoic–Cenozoic sandstones at depths of 3500–6000 m are within phase A of the middle diagenetic stage. Silica, kaolinite, and chlorite are the dominant

cements in the Triassic–Jurassic sandstones. Carbonates are the dominant cement in the Cretaceous and Paleogene sandstones, whereas evaporite cements are also important in the Paleogene sandstones.

2) The Late Jurassic was characterized by a pronounced regional climatic transition. The Triassic–Early Jurassic climate was warm and humid, and characterized by extensive lacustrine and swamp facies environments, with reducing and acidic water conditions. In contrast, the Cretaceous–Paleogene was characterized by arid conditions. Cretaceous sediments were mainly deposited in lacustrine and deltaic facies under freshwater to brackish water conditions, and the Paleogene sediments were deposited in tidal flat and saline lake facies under alkaline water conditions.

3) Climate change and marine transgressions caused variations in the water chemistry during the deposition of the Triassic–Jurassic, Cretaceous, and Paleogene sediments, directly influencing the distinct diagenetic types observed in each period.

Acknowledgements

This paper is dedicated to the memory of Dr Juan Li. This paper benefited from enlightening discussions with Yi Gu, Yixiong Qian, Chengshan Jia, Wei Yao, Huixi Lin, Yukai Qi, Jie Xu, and Fusong Luo. We are deeply grateful to the editor and reviewers for their constructive and helpful suggestions. This study was supported financially by the National Natural Science Foundation of China (No. 42102120), the Sinopec Project (No. KY2018-S-077), a doctoral research start-up fee of Henan Normal University (No. 20220091), and the Natural Science Foundation of Henan (No. 202300410241).

References

Ajdukiewicz, J. M. & Lander, R. H. (2010) Sandstone reservoir quality prediction: The state of the art. *AAPG bulletin*, 94 (8), 1083–1091. https://doi.org/10.1306/intro060110

Bjørlykke, K. (1983) Diagenetic Reactions in Sandstones. *Sediment Diagenesis*, 115, 169–213. https://doi.org/10.1007/978-94-009-7259-9_3

Bjørlykke, K. (2014) Relationships between depositional environments, burial history and rock properties. Some principal aspects of diagenetic process in sedimentary basins. *Sedimentary Geology*, 301, 1–14. https://doi.org/10.1016/j.sedgeo.2013.12.002

Chen, L., Lin, C., Li, H. & Xiang, S. (2017) Sedimentary characteristies of the lower sandstone part of Kumugeliemu group in the western Tabei uplift. J*ournal of Northeast Petroleum University*, 41 (5), 23–32. https://doi.org/10.1016/j.sedgeo.2013.12.002

Compiling Group for Xinjiang Regional Stratigraphic Chart (1981) *Regional stratigraphic chart of northwestern China, branch of Xinjiang Uygur Autonomous Region*. Geological Publishing House, Beijing, 496 pp. [In Chinese]

Fuchtbauer, H. (1983) Facies controls on sandstone diagenesis. *Sendiment diagenesis*, 115, 269–288. https://doi.org/10.1007/978-94-009-7259-9_5

Garzanti, E. (2019) Petrographic classification of sand and sandstone. *Earth Science Reviews*, 192, 545–563. https://doi.org/10.1016/j.earscirev.2018.12.014

Gu, J.Y., Jia, J.H. & Fang H. (2002) Reservoir characteristics and factors of high porosity and permeability in the Tarim Basin. *Chinese Science Bulletin*, 47, 9–15. [In Chinese] https://doi.org/10.1007/BF02902813

Han, D.L, Li, Z, Han, Y.X., Liu, J.Q, Li, W.F. & Li, S.L. (2009) Sealing feature of burial diagenesis environment and its controls on differentiation of cementation in Cretaceous sandstone reservoir in Kelasu structure zone, Kuqa depression. *Acta Petrologica Sinica*, 25 (1), 2351–2362. [In Chinese]

Hendrix, M.S., Graham, S.A., Carroll, A.R., Sobel, E.R., McKnight, C.L., Schulein, B.J. & Wang, Z. (1992) Sedimentary record and climatic implications of recurrent deformation in the Tian Shan: Evidence from Mesozoic strata of the north Tarim, south Junggar, and Turpan basins, northwest China. *Geological Society of America Bulletin*, 104 (1), 53–79. https://doi.org/10.1130/0016-7606(1992)104<0053:SRACIO>2.3.CO;2

Huang, S.J., Huang, K.K., Feng, W.L., Tong, H.P., Liu, L.H. & Zhang, X.H. (2009) Mass exchanges among feldspar, kaolinite and illite and their influences on secondary porosity formation in clastic diagenesis—a case study on the Upper Paleozoic, Ordos Basin and Xujiahe Formation, Western Sichuan Depression. *Geochimica*, 38 (5), 498–506. [In Chinese]

Jia, C.Z. & Pang, X.Q. (2015) Research processes and main development directions of deep hydrocarbon geological theories. *Acta Petrolei Sinica*, 36 (12), 1457–1469. [In Chinese]

Jin, X.H., Yan, X.B., Li, T.J. & Zou, Y.R. (2008) A discussion on gas and oil exploration activities and discovery patterns in the Tarim Basin. *Oli & Gas Geology*, 4 (1), 45–52. [In Chinese]

Li, W.G., Zhang, X.P. & Zhong, Y.M. (2005) Formation mechanism of secondary dissolved pores in arcose. *Oli & Gas Geology*, 26 (2), 220–223. [In Chinese]

Li, Z., Song, W., Peng, S., Wang, D. & Zhang, Z. (2004) Mesozoic–Cenozoic tectonic relationships between the Kuqa subbasin and Tian Shan, northwest China: constraints from depositional records. Sedimentary Geology, 172 (3-4), 223–249. https://doi.org/10.1016/j.sedgeo.2004.09.002

Li, Z., Chen, J.S. & Guan, P. (2006) Scientific problems and frontiers of sedimentary diagenesis research in oil-gas-bearing basins. *Acta Petrologica Sinica*, 22 (8), 2113–2122. [In Chinese]

Liu, J.D., Qi, L.X., Tian, J.C., Li, Z.J. & Zhang, X.B. (2014) *Tectonic evolution and sedimentary framework of the Tarim Basin*. Chinese Science Publishing House, Beijing, 346 pp. [In Chinese]

Luo, J.L., Li, C., Lei, C., Cao, J.J. & Song K.P. (2020) Discussion on research advances and hot issues in diagenesis of clastic-rock reservoirs. *Journal of Paleogeography*, 22 (6), 1021–1040. [In Chinese]

McLennan, S. M. (2001) Relationships between the trace element composition of sedimentary rocks and upper continental crust. *Geochemistry, Geophysics, Geosystems*, 2 (4). https://doi.org/10.1029/2000GC000109

Morad, S., Al-Ramadan, K., Ketzer, J.M. & De Ros, L.F. (2010) The impact of diagenesis on the heterogeneity of sandstone reservoirs: A review of the role of depositional facies and sequence stratigraphy. *AAPG bulletin*, 94 (8), 1267–1309. https://doi.org/10.1306/04211009178

Muhs, D.R., Bettis, E.A., Been, J. & McGeehin, J.P. (2001) Impact of climate and parent material on chemical weathering in loess-derived soils of the Mississippi River valley. *Soil Science Society of America Journal*, 65 (6), 1761–1777. https://doi.org/10.2136/sssaj2001.1761

Qi, L.X., Li, Z.J. & Lv, H.T. (2020) *Atlas of tectonic-sedimentary evolution and hydrocarbon exploration in the Tarim Superimposed Basin*. Chinese Science Publishing House, Beijing, 224 pp. [In Chinese]

Qiu, L.W., Jiang, Z.X., Cao, Y.C., Qiu, R.H. & Chen, W.X. (2001) Alkaline diagenesis and its influence on a reservoir in the Biyang Depression. *Science in China Series D: Earth Sciences*, 31 (9), 752–759. [In Chinese] https://doi.org/10.1360/02yd9065

Singer, A. (1984) The paleoclimatic interpretation of clay minerals in sediments—a review. *Earth-Science Reviews*, 21 (4), 251–293. https://doi.org/10.1016/0012-8252(84)90055-2

Sun, D.Q., Li, W.H., Lu, S.F., Liu, X.P, He, T.H., Zhu, P.F., Wang, X.Z, Ying, J.F. & Wang, J.M. (2020) Reservoir characteristics and controlling faceors of Shushanhe Formation on Yingmaili Area of Tabei Uplift. *Journal of Northeast Petroleum University*, 44 (6), 82–93. [In Chinese]

Tang, T.F., Xue, Y.S. & Yu, C.L. (1992) *Marine Sedimentary Characteristics and Environments from Late Cretaceous to Early Tertiary in the West Part of Tarim Basin of Xinjiang*. Chinese Science Publishing House, Beijing, 175 pp. [In Chinese with English abstract]

Tian, J.F., Chen, Z.L., Fan, Y.F., Li, P.P. & Song, L.J. (2008) The occurrence, growth mechanism and distribution of authigenic chlorite in sandstone. *Bulletin of Mineralogy, Petrology and Geochemistry*, 27 (2), 200–206. [In Chinese]

Tribovillard, N., Algeo, T.J., Lyons, T. & Riboulleau, A. (2006) Trace metals as paleoredox and paleoproductivity proxies: an update. *Chemical geology*, 232 (1-2), 12–32. https://doi.org/10.1016/j.chemgeo.2006.02.012

Wu, G.K., Lin, C.S., Liu, Y.F., Liu, J.Y., Yang, X.Z. & Li, H. (2019) Characteristics of major unconformities and paleo-geomorphology during the Mesozoic key transformation stages in Kuqa-Tabei area. *Oil & Gas Geology*, 40 (4), 763–777. [In Chinese]

Xia, Y.T., Wang, R., Yang, H.C., Shi, W.Z., Bahetiyaer, A., Tan, S., Zhang, X. & Xu, Z. (2024) Characteristics and main controlling factors of the tight sandstone reservoirs around the paleo-uplift in the southern Tianshan area, Tarim Basin. *Bulletin of Geological Science and Technology*, 43 (2), 16–27. [In Chinese]

Xie, X.N., Cheng, J.M. & Meng, YL. (2009) Basin fluid flow and associated diagenetic processes. *Acta Sedimentologica Sinica*, 27 (5), 863–871. [In Chinese with English abstract]

Xu, X.H., Zhou, Q.F. & Zhang, L. (2004) Oil and gas reserves and their distribution in Tarim basin. *Oil & Gas Geology*, 25 (3), 300–313. [In Chinese]

Xu, Y., Cao, Y., Liu, C., Zhang, H. & Nie, X. (2020) The history of transgressions during the Late Paleocene-Early Eocene in the Kuqa Depression, Tarim Basin: constraints from COS-Sr isotopic geochemistry. *Minerals*, 10 (9), 834 pp. https://doi.org/10.3390/min10090834

Yang, H.J., Liu, Y.F., Su, Z. & Han, J.F. (2020) The main controlling factors for the formation of high quality clastic reservoirs in deeply buried strata of Tabei Uplift. *Geological Review*, 66 (1), 169–179. [In Chinese with English abstract]

Yang, Y.T., Guo, Z.X. & Luo, Y.J. (2017) Middle-Late Jurassic tectonostratigraphic evolution of Central Asia, implications for the collision of the Karakoram-Lhasa Block with Asia. *Earth-Science Reviews*, 166, 83–110. https://doi.org/10.1016/j.earscirev.2017.01.005

Yi, Z.Y., Liu, Y.Q. & Meert, J.G. (2019) A true polar wander trigger for the Great Jurassic East Asian Aridification. *Geology*, 31 (2), 1112–1116. https://doi.org/10.1130/G46641.1

Ying, F.X., He, D.B., Long, Y.M. & Lin, X.S. (2003) Division of clastic diagenetic stage (SY/T 5477-2003). State economic and trade commission. [In Chinese]

Yu, B.S. & Lai, X.Y. (2006) Carbonic acid system of groundwater and the solubility of calcite during diagenesis. *Acta Sedimentologica Sinica*, 24 (5), 627–635. [In Chinese]

Zhang, R.H., Zeng, Q.L., Li, J., She, M. & Yu, C.F. (2019) Physical Simulation of Multi-Period Dissolution in Cretaceous Reservoirs of Kelasu Tectonic Belt, Kuqa Depression. *Xinjiang Petroleum Geology*, 40 (1), 34–40. [In Chinese with English abstract]

Zhang, R.H., Zou, W.H., Chen, G, Zhao, J.L., Zhang, H.L., Wu, J. & Li, X.J. (2018a) Characteristics and hydrocarbon exploration significance of the huge Lower Cretaceous lacustrine sand bar in the northern Tarim Basin. *Acta Petrolei Sinica*, 39 (8), 845–857. [In Chinese]

Zhang, S.J., Hu, X.M., Han, Z., Li, J. & Garzanti, E. (2018b) Climatic and tectonic controls on Cretaceous-Palaeogene sea-level changes recorded in the Tarim epicontinental sea. *Palaeogeograpy, Palaeoclimatology, Palaeoecology*, 501, 92–110. https://doi.org/10.1016/j.palaeo.2018.04.008

Zheng, J.M. & Ying, F.X. (1997) Reservoir characteristics and diagenetic model of sandstone intercalated in coal-bearing strata (acid water medium). *Acta Petrolei Sinica*, 18 (4), 19–24. [In Chinese]

Zhu, R.K., Guo, H.L., Gao, Z.Y., Han, D., Zhang, L.J., Sun, Y.S. & Cheng, M. (2007) Probe into influence factors to the physical properties of the Cretaceous and Eocene reservoir in northern Tarim Basin. *Geological Review*, 53 (5), 624–630. [In Chinese]

Zhou, Z. (2001) *Stratigraphy of the Tarim Basin*. Chinese Science Publishing House, Beijing, 359 pp. [In Chinese]

All Supplementary materials are available at:
https://doi.org/10.11646/mesozoic.1.3.21

Supplementary materials:

Supplementary Info 1—Detrital composition, Interstitial minerals and Porosity

Supplementary Info 2—Clay minerals